Exposure characteristics of cobalt fluoride (CoF_2) self-developing electron-beam resist on sub-100 nm scale

Marek Malac,[a] Marvin Schoefield, and Yimei Zhu
Building 480, Brookhaven National Laboratory, Upton, New York 11973

Ray Egerton
Department of Physics, University of Alberta, Edmonton T6G 2J1, Canada

(Received 15 October 2001; accepted for publication 26 April 2002)

We have studied electron-beam exposure of cobalt fluoride (CoF_2) thin films by real-time high-resolution transmission electron microscopy and by electron energy-loss spectroscopy. We were able to remove fluorine completely from an irradiated area and retain metallic cobalt by exposing the area at low dose rate and elevated temperature. The structures were composed of separated single-crystal cobalt nanoparticles with dimensions on the order of 5–10 nm. © *2002 American Institute of Physics.* [DOI: 10.1063/1.1487914]

I. INTRODUCTION

As the scaling limit of silicon based microelectronic devices is approached the need for a new generation of signal processing and storage device becomes more urgent. One possibility is a device based on propagation of magnetic excitations through chains of coupled magnetic particles.[1] The magnetic storage industry faces a similar scaling challenge. As the storage density (bits/in.^{2}) increases, the magnetic properties of individual magnetic nanoparticles, coupling between individual particles arranged in an array, as well as magnetic reversal of such particles becomes technologically important. Additionally, understanding the behavior of magnetic particles and arrays of such particles on a mesoscopic length scale (characteristic dimensions <100 nm) presents a challenging question in modern physics.[2] The above possibilities, along with the wide variety of existing magnetic devices and sensors, makes magnetism on a nanometer scale a very active research field in both basic and applied directions.

A first step in the quest for urgently needed experimental data is a reliable method for fabrication of magnetic structures on a few nanometer length scales. From a more practical point of view such a fabrication method is essential for prototyping and testing of devices. The need for a well-defined wide variety of shapes of such structures as well as the capability of determining the position of the structures suggests the use of lithographical techniques rather than chemical and self-assembly methods. Transition metal halides are promising high-resolution self-developing electron beam resists for this task.[3] For magnetic applications cobalt fluoride (CoF_2) and iron fluoride (FeF_2) are perhaps the most promising materials.[3] These fluorides offer the possibility of direct writing of cobalt or iron structures on a few nanometer length scale without the need of an additional postexposure processing. Scanning tunneling microscope is an alternative tool for fabrication on atomic scale,[4,5] but is too slow for fabrication of structures with characteristic dimensions on the order of several nanometers.

A second essential step is the capability of mapping the spatial distribution of magnetic potential in such structures and arrays of such structures. Kerr microscopy provides a method for retrieving magnetization distribution in thin magnetic films.[6] Additionally, Kerr microscopy allows for experimental studies of time-dependent processes, such as magnetic reversal.[7,8] Magnetic force microscopy (MFM) also provides a way to characterize magnetic samples, however the spatial resolution limit is currently on the order of ~ 25 nm and the technique is sensitive only to fringing field.[9] The sensitivity of MFM to topographical contrast presents an additional challenge for correct interpretation of the data. Methods based on the phase change of an electron wave passed through a region with nonzero magnetic vector potential[10] offer several advantages. First, measurements of weak magnetic fields can be realized.[11] Second, the method is sensitive to both magnetization within a sample as well as fringing fields.[12] Experimentally such measurement of an electron wave phase can be realized in a transmission electron microscope (TEM). Spatial resolution of phase mapping in TEM can be as good as a few nanometers[12] with the objective lens of the TEM turned off (as required of mapping of sample magnetization). Off-axis electron holography is a suitable method for *quantitative* measurement of the electron phase.[13]

The use of a self-developing electron-beam resist in the TEM for fabrication of magnetic nanostructures combined with electron holography for magnetic potential measurements offers the possibility of *in situ* fabrication and characterization of samples. At the same time the analytical capabilities of the TEM can be used to characterize chemical and structural properties and study the exposure process.

In this article we discuss the mechanism and limitations of electron-beam exposure of cobalt fluoride thin films and challenges involved in using this material as an electron-beam resist. Different substrates and a wide range of exposure conditions were used in this study. The exposure process

[a]Author to whom correspondence should be addressed; electronic mail: mmalac@phys.ualberta.ca

and resulting patterns were characterized by electron energy loss spectroscopy (EELS) and high-resolution transmission electron microscopy (HRTEM). Additionally, HRTEM used for *real-time* observation (and recording) of the processes *within* the exposing probe provides valuable insight into cobalt thin-film growth on nearly atomic scale.

II. SPECIMEN PREPARATION

We have used an ion-pumped ultrahigh vacuum (UHV) system to deposit thin films of CoF_2 (Alfa Aesar No. 13074) from a resistively heated molybdenum boat. To prevent deposition of hydrates[3] as well as to outgas the source material, the latter was preheated at approximately 200 °C for several days. The pressure in the deposition system was typically in the low 10^{-8} Torr range prior to deposition, and stayed typically in the low 10^{-7} Torr range during deposition. The films were deposited at a growth rate 0.04–0.13 nm/s onto a room-temperature substrate. Film thickness was monitored during deposition by a crystal film thickness monitor. Total film thickness was typically between 15 and 30 nm. As a substrate we used 10 nm thick amorphous carbon film stretched on 200-mesh TEM grids for most experiments. Additionally, ion-milled single-crystal germanium and 45 nm thick C_{60} films stretched on 200-mesh TEM grids were used to determine the influence of the substrate material. After CoF_2 deposition the samples were transferred directly to an electron microscope, keeping the exposure to laboratory air to less than 10 min.

III. CHARACTERIZATION

We have used a JEOL 3000F field-emission TEM equipped with Gatan Image Filter™ (GIF) for EELS and energy-filtering TEM (EFTEM). We have used the TV-rate camera below the GIF spectrometer for recording a real-time high-resolution TEM movie of the processes *within* the area exposed by the electron beam (5–100 nm in diameter). Heating and cooling sample stages allowed us to study the exposure process at temperatures between 85 and 700 K. The EELS spectra for quantitative measurements of fluorine removal were collected in the nanobeam diffraction mode of the TEM. The probe diameters were between 30 and 500 nm and the EELS collection semiangle was 1.5 mrad, defined by the spectrometer entrance aperture and appropriate camera length. We have studied the exposure process at temperature $T=85$ K, $T=293$ K, $T=380$ K, $T=555$ K, and $T=697$ K. The dose rate j (beam current per unit area) was varied over more than 4 orders of magnitude (from about 0.1 to about 1200 A/cm^2). We measured the beam current using readings of the TEM screen based on Faraday cup calibration. The beam current was stable within the accuracy ($\sim$0.01 A/cm^2) of the beam-current measurements throughout the experiments. Pattern writing was achieved via the internal programming language of the JEOL 3000F electron microscope and, for real-time recording of the exposure process, by moving the sample with respect to a stationary electron beam.

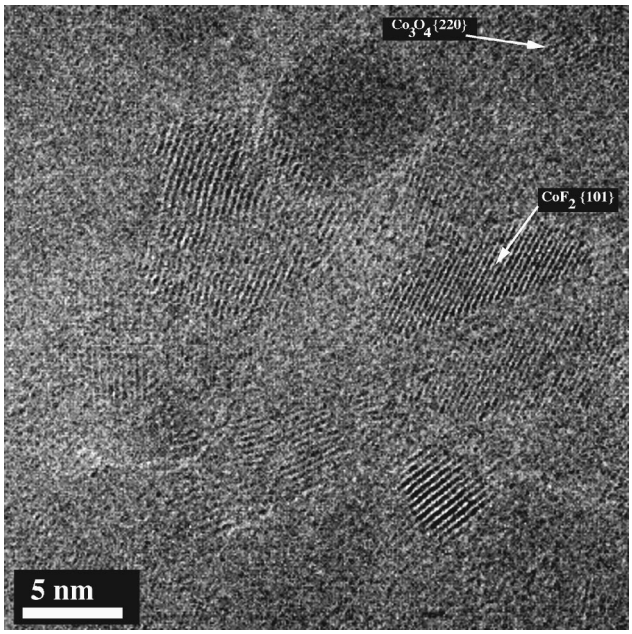

FIG. 1. Initial cobalt fluoride (CoF_2) film on 10 nm thick amorphous carbon substrate, the CoF_2 film thickness is 15 nm. Area of Co_3O_4 with planes {220} parallel to the electron beam direction and area of CoF_2 with {101} planes parallel to the beam direction are marked by arrows. The scale bar corresponds to 5 nm.

IV. RESULTS

A. Real-time HRTEM observations

A TEM of initial cobalt fluoride film deposited on amorphous carbon substrate is shown in Fig. 1. The figure shows that the initial films were continuous (with no voids) and nanocrystalline. The somewhat brighter crystallite boundaries have developed during the image acquisition and are characteristic of the initial stages of CoF_2 exposure by the electron beam. The lack of voids in the initial CoF_2 film does not confirm that the CoF_2 film is flat on atomic scale; more likely, the film may be rough on length scale comparable to or smaller than the crystallite size.[14,15] That is between $\sim$2 and $\sim$7 nm for a 15–20 nm thick cobalt fluoride film. As expected for a thin film deposited under conditions of low adatom diffusion (low substrate temperature T_s) the crystallite size did not depend on the substrate material.[14] Quantitative EELS (see Ref. 16, page 277) revealed the composition of the initial film to be stoichiometric CoF_2 within the accuracy of EELS measurements (which we estimate to be $\sim$10%).

Electron exposure resulted in progressively lower fluorine concentration. The microscopic mechanism of this exposure process determines the microstructure and properties of the final cobalt patterns. We therefore summarize real-time observations of the electron-beam exposure as follows: The exposure proceeds in several distinct steps. First, at doses of about 50 C/cm^2 or less (at room temperature) the grain boundaries within exposed areas become more ''visible'' or developed, such as in Fig. 1. This step proceeds at approximately the same rate within the whole area illuminated by the electron beam. The time duration of this step decreases with increasing substrate temperature and with increasing

dose rate. The initial cobalt particle size identified in the high-resolution images is on the order of 2 nm, which may be interpreted as the upper limit of critical nuclei diameter. Such small, round nuclei are visible at all temperatures and dose rates used. These initial nuclei are often formed at CoF_2 crystallite boundaries and triple junctions of crystallite boundaries, possibly due to faster fluorine depletion in these areas. Initial nuclei are also formed away from crystallite boundaries (grain interior) of the initial CoF_2; their size does not appear to be larger than those formed at the crystallite boundaries or triple junctions. When the diameter illuminated by the electron beam is larger than about 10 nm, multiple nuclei are formed, but not simultaneously within the whole illuminated area. When the beam diameter is small (~ 3 nm) the initial nuclei tend to form *outside* the central area of the electron beam. The relatively small dose (~ 50 C/cm^2 at room temperature) required for formation of the nuclei suggests that they can be readily formed within the beam tails, in places with more favorable local conditions (grain boundary, local supply of cobalt atoms, local temperature, etc.). The formation of Co crystallites on the perimeter of the electron beam becomes more pronounced with increase of the dose rate j and almost no cobalt forms within the central portion of the electron beam at $j > 1200$ A/cm^2. There are many possible explanations for this suppressed cobalt formation within the high intensity beam. First, the high current density can lead to removal of cobalt by the knock-on mechanism. Second, the knock-on mechanism may increase the kinetic energy of the released cobalt atoms at the CoF_2 surface, resulting in decreased condensation rates within the high-current density area. It is also possible that the high current density j and consequent high rate of CoF_2 removal leads to a fast changing CoF_2–Co interface. Such an interface can again reduce the condensation rates for cobalt within the central portion of the electron beam. The influence of electric field on removal of material from the central portion of the beam was discussed by Humphreys and Chen.[17] Zanetti *et al.*[18] discussed the influence of gas bubble formation on the exposure characteristics of alkali halides. From our calculations [Eq. (9)] it appears that the knock-on mechanism alone is not likely to explain the complete removal of both fluorine and cobalt from the central portion of the beam. Based on our observations it is however difficult to exclude any of the remaining explanations.

The exposure process then proceeds by growth of the cobalt nuclei. At first, these nuclei are round but they become faceted crystallographically as the size of the crystallites increases. The round shape of the initial nuclei and small crystallites may be induced by a radially symmetric supply of cobalt atoms. In other words, the cobalt atoms, once liberated from the CoF_2 film, diffuse within the film plane from all radial directions toward a cobalt nucleus, which acts as a trap for free cobalt atoms within the diffusion distance of the nuclei, creating a cobalt concentration gradient in the film plane (Ref. 17, page 8–15). When the same area is exposed further, the faceted crystallites reach a size of about 10–20 nm. Such faceted crystallites often have an elongated shape, presumably determined by the orientation of fast-growing crystal planes and local growth conditions. Figure 2 shows

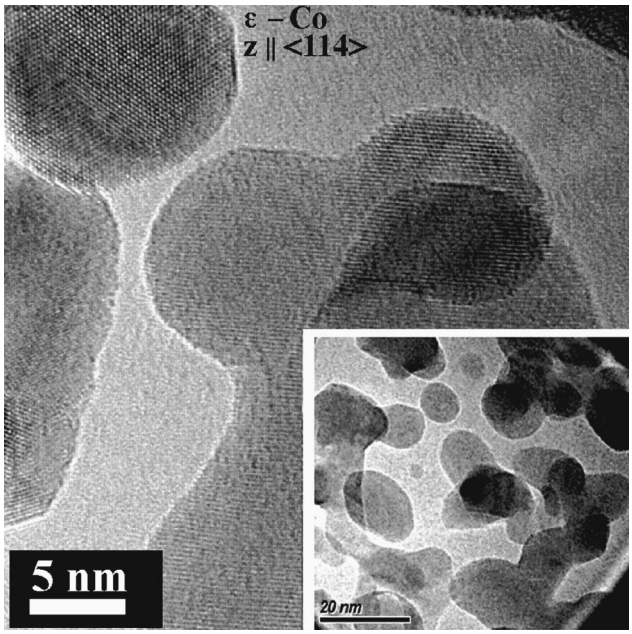

FIG. 2. High resolution image of partially exposed area with overlapping crystallites. The area was exposed at $T = 550$ K and $j = 11$ A/cm^2. The area was exposed to ~ 1200 C/cm^2. Large particle in the upper left corner is ?-cobalt with $\langle 114 \rangle$ zone axis oriented parallel to the electron beam direction. The scale marker corresponds to 5 nm. (Inset) Low magnification of a nearby area under similar exposure conditions. Scale bar corresponds to 20 nm.

the beginning of the faceting stage. In this figure the cobalt crystallites overlap (inset), but do not coalesce despite the elevated substrate temperature ($T \sim 550$ K) and prolonged exposure to the electron beam (> 1200 C/cm^2). There is also remaining CoF_2 present near the cobalt crystallites. The average size of the cobalt crystallites in Fig. 2 (inset) is much larger than the size of the initial CoF_2 crystallites (Fig. 1). This large size suggests that the supply of cobalt atoms to a growing cobalt crystallite extends beyond the size of an initial CoF_2 crystallite.

Further exposure by the electron beam leads to only a slight increase of the cobalt crystallite size. However, existing cobalt crystallites often change their projected shape, retaining the facetted overall look but changing the configuration of the facets. During this shape change parts of the cobalt particles often move (sweep) across any unexposed cobalt fluoride film that may be still present. In many cases a new cobalt nucleus forms in an area swept by a large cobalt grain as well as within an area overlapping with an existing Co particle. Such nuclei follow the growth evolution described above. The result is a film composed of individual, but often overlapping, cobalt crystallites on a bare substrate. At extremely large doses, larger cobalt particles grow at the expense of smaller particles. This coarsening (ripening) process seems to reach saturation at about 40 nm crystallite size. Crystallites similar to those found at the initial stage (round and less than 5 nm in diameter) are often found between the large ones. At the end of this ripening stage no CoF_2 was seen in the HRTEM micrographs and no fluorine was detectable by EELS.

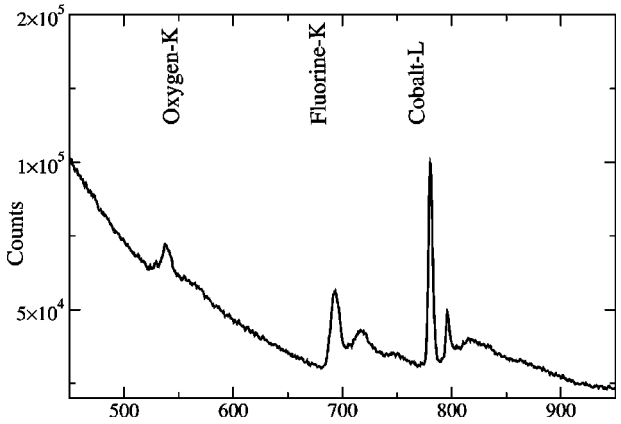

FIG. 3. Typical "as prepared" electron energy loss spectrum collected at $T=85$ K and dose rate $j=0.1$ A/cm^2. The fluorine to cobalt atomic ratio is F/Co=2 corresponding to stoichiometric CoF_2.

The increase of the cobalt crystallite size with time (at given temperature and dose rate j) can provide information on diffusion processes governing the growth of the crystallites. Namely, if the diffusion follows the relation

$$dx = Ct^m, \tag{1}$$

(where dx is the increase of size of the cobalt particle, C and m are constants, and t is time) then the exponent m can reveal whether surface (boundary) or bulk diffusion governs the growth process. The measured values of the exponent m for different crystallites vary between 0.17 and 0.34 (exposed at $T=547$ K and $j=18$ A/cm^2). The measurements were undertaken from the very initial stage of the crystallite appearance, from 2 to about 7 nm in size. The exponents therefore should provide information on the initial stages of cobalt crystallite growth rather than on the ripening stage. The value of the exponent $m=1/3$ indicates a bulk diffusion controlled process, while $m=1/4$ indicates boundary diffusion controlled process.[18] Our measured values suggest that both bulk and boundary diffusion processes can be important. The measured value of $m=0.17$ suggests the existence of a mechanism inhibiting the diffusion of cobalt atoms (such as contamination buildup).

B. Result of EELS measurements and EFTEM chemical mapping

Results of EELS measurements are presented in this section. As mentioned above, the EELS spectra were acquired in the diffraction mode of the electron microscope. In this mode, the spectrum is collected from the whole illuminated area of the specimen, thereby avoiding complications arising from chromatic aberration (Ref. 16, page 75). Quantitative measurements of F/Co atomic ratios were obtained by integrating the fluorine K loss and cobalt L loss intensities over a 50 eV window and weighting by the appropriate inelastic cross sections. The inelastic cross sections were calculated by SIGMAK3 and SIGMAL3 programs (Ref. 16, page 420) for K and L edges, respectively. A typical core-loss spectrum of an as-prepared specimen (atomic ratio F/Co=2 with estimated accuracy $\sim 10\%$) is shown in Fig. 3. The removal of fluorine from the initial CoF_2 film can be described in terms of a characteristic dose D_e: the dose at which the number of fluorine atoms decreases to $1/e$ of the initial value (Ref. 16, page 392). The dependence of D_e on temperature and dose rate j can yield information on the irradiation processes involved. Our measured characteristic doses D_e for different dose rates and temperatures of the exposure are in Table I. The increase of the characteristic dose with increased dose rate can be attributed to diffusion-limited removal of fluorine from the CoF_2 film.[19] Similar behavior was observed for exposures done at room temperature ($T=293$ K) and $T=555$ K. The characteristic dose D_e for a given dose rate j decreases with increasing temperature T. This decrease of D_e is a result of several competing processes and will be discussed in the next section. EELS experiments revealed the presence of oxygen in all samples: both as prepared and after exposure. To determine whether the oxygen is present as a cobalt oxide, water–ice adsorbed on the sample or a hydride of CoF_2 we carried electron diffraction experiments described below.

TABLE I. Measured characteristic doses D_e for different dose rates j and substrate temperatures during exposure.

Substrate temperature T (K)	Dose rate j j (A/cm2)	Characteristic dose D_e (C/cm^2)
85	0.1	8500
85	2.8	10 200
85	30	11 400
85	1,200	433 000
293	0.2	520
293	17	14 600
380	18	4000
555	0.1	27
555	28	400
697	0.1	9

EFTEM provides a convenient way to determine thickness variations (Ref. 16, page 302) and spatial distribution of cobalt and fluorine within an exposed area (Ref. 16, page 330). Figure 4 (acquired at room temperature) shows the changes in the thickness and elemental composition of an exposed area [marked with a rectangle in Fig. 4(a)]. The thickness map in Fig. 4(b) confirms that the cobalt crystallites are thicker than the nearby unexposed CoF_2. A fluorine map [Fig. 4(c)] reveals depletion of fluorine coincident with the cobalt particles. The cobalt map [Fig. 4(d)] suggests depletion of cobalt from the areas adjacent to the cobalt crystallites. Thickness maps, such as in Fig 4(b), can also be used to obtain additional information on the growth of the cobalt particles. Figure 5 shows measured cobalt particle thickness as a function of projected particle diameter (as seen in TEM micrographs). The thickness was measured just prior to the ripening stage of the exposure process. The increase of the cobalt particle thickness with its projected size suggests a three-dimensional growth process, however the particles are typically disc like with an aspect ratio (thickness/projected size) slightly less than one (solid line in Fig. 5).

C. Results of electron diffraction experiments

Diffraction experiments can reveal the structure of the metallic cobalt nanoparticles. The structure of metallic cobalt

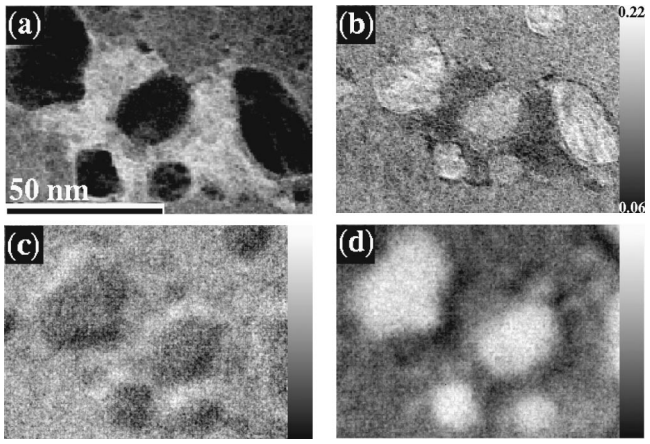

FIG. 4. (a) Zero loss filtered image of partially exposed CoF_2 film. The area marked by the rectangle was exposed by a focused electron beam prior to the acquisition of the images. The scale bar corresponds to 50 nm; (b) thickness map, scaled in units of inelastic mean free path (MFP), the substrate thickness (0.1 MFP of amorphous carbon) was subtracted; (c) fluorine map; and (d) cobalt map of the area marked in (a). The brighter areas correspond to thicker sample in (b), more fluorine in (c) and more cobalt in (d).

nanoparticles presents an intriguing question since the hcp structure of bulk cobalt can change to fcc as the size of the particles decreases.[20] Metallic cobalt nanoparticles with a simple cubic structure (ϵ-cobalt) have also been observed.[21] We have also undertaken selected-area electron-diffraction experiments to determine whether cobalt oxide (CoO, Co_2O_3, and Co_3O_4) was present. Our diffraction experiments were carried out at different substrate temperatures, on pristine (as-prepared CoF_2) samples, and on exposed samples at the beginning of the ripening stage. The DPs were acquired from the exposed area typically ~ 500 nm in diameter at a dose rate ~ 0.2 A/cm^2 at two different acquisition times (0.25 and 1 s) such that low index as well as high index and weak reflections can be observed. The diffractograms of as-prepared CoF_2 film (total dose for acquisition of diffraction patterns $D < 3.6$ C/cm^2) confirm the presence of CoF_2 as well as detectable fractions of CoF_3, CoO, Co_2O_3, Co_3O_4, and ϵ-cobalt. The diffractograms acquired from areas exposed at room temperature with $j = 2$ A/cm^2 to a dose $D = 380$ C/cm^2 revealed the presence of ϵ-cobalt as well as CoF_2, CoF_3, CoO, and Co_3O_4. The presence of the remaining metallic cobalt structures (fcc-Co or hcp-Co) could not be confirmed or excluded, because only reflections overlapping those of other compounds were present. The diffraction patterns did not contain reflections corresponding to Co_2O_3. The areas exposed at $T = 554$ K with dose rate $j = 0.8$ A/cm^2 and dose $D = 450$ C/cm^2 confirmed the presence of metallic cobalt in at least one of the possible structures (fcc-Co, hcp-Co, and ϵ-cobalt). Detectable amounts of CoF_2, CoO, and Co_3O_4 were also present.

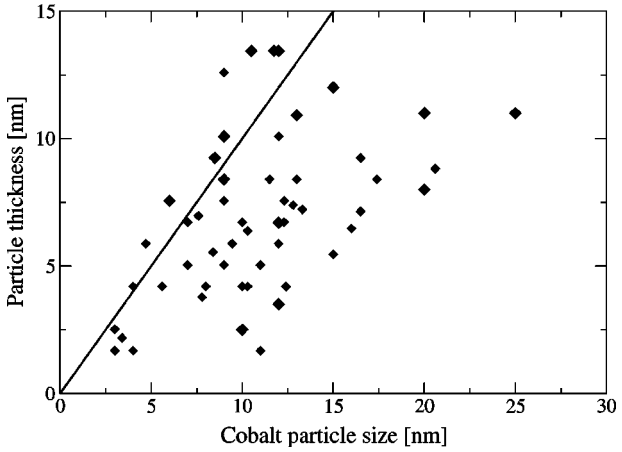

FIG. 5. Relation between measured projected particle size (diameter) and measured particle thickness for particles just before ripening stage. The solid line corresponds to aspect ratio (height/diameter) = 1. Most cobalt particles have aspect ratio slightly less than one.

The above investigations should be considered in the context of the chemistry of cobalt. Bulk cobalt is prone to oxidation (Ref. 22, page 127). In bulk materials Co_3O_4 is found at fully oxidized surfaces while CoO is found close to the unoxidized metal and is susceptible to further oxidation. Even at 100 °C the presence of oxygen leads to the formation of Co_3O_4.[22] The presence of adsorbed oxygen and water may be unavoidable even in an UHV TEM since the samples are exposed to laboratory air during transfer from the growth chamber, so the possibility of formation of oxides needs to be taken into account. This explains the presence of cobalt oxides detected in diffraction patterns.

V. DISCUSSION

As stated at the outset, the aim of this article is to study the formation of cobalt structures and consequences of the formation process on the suitability and resolution of CoF_2 as an electron-beam resist. We therefore refrain from comments on the interaction of fast electrons with CoF_2 and on the fluorine desorption mechanism. Chen and Humphreys[17] provide a detailed discussion of the electron-beam interactions with fluorides and Ref. 23 discusses the fluorine desorption mechanism in great depth. A qualitative model of the exposure process is presented in next Sec. V A.

A. Qualitative model for CoF_2 removal and cobalt particle formation

A simplified model of CoF_2 exposure is schematically depicted in Fig. 6. First, as the initial CoF_2 film is exposed to the electron beam fluorine is removed from the surface layer and cobalt nuclei start to form [Fig. 6(a)]. As the exposure proceeds, these nuclei grow at the expense of the underlying CoF_2. The growing cobalt nuclei prevent fluorine escape from the underlying CoF_2 film, but do not prevent fluorine escape from adjacent areas. At the same time, the cobalt nucleus collects cobalt atoms liberated from CoF_2 within a diffusion distance. Consequently, the CoF_2 film is removed faster between the Co nuclei than underneath such nuclei, and nuclei end up at different heights relative to the substrate. This leads to an increase of the distance a liberated cobalt atom has to travel to reach a cobalt nucleus. Eventually liberated cobalt atoms will reach a sufficiently high concentration to form a new nucleus at a level closer to the substrate [Fig. 6(b)]. Since this new nucleus is formed at a different height, it can overlap with the initial nuclei in a

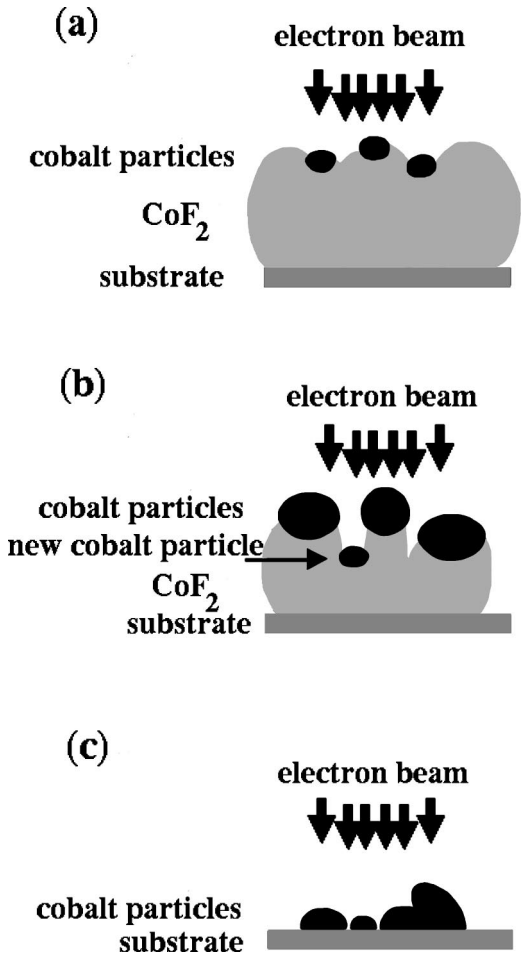

FIG. 6. Cartoon of exposure process: (a) formation of initial cobalt nuclei on pristine CoF_2 film; (b) initial cobalt nuclei are higher above the substrate than a newly forming cobalt nucleus (marked by an arrow) leading to overlap of the new cobalt nucleus with the nuclei started in (a); and (c) exposed film at the beginning of the ripening stage. The (partially overlapping) cobalt particles are on a bare substrate and the CoF_2 is removed completely.

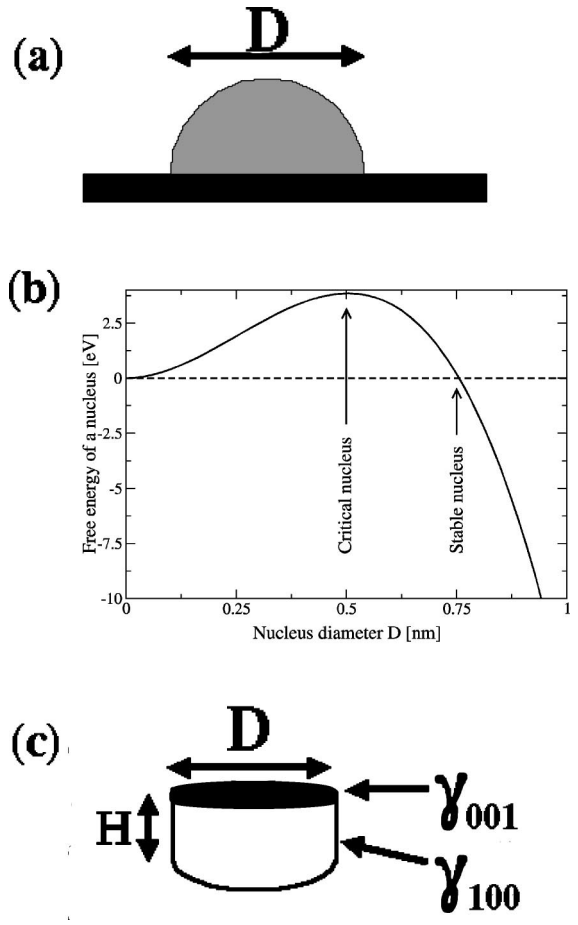

FIG. 7. (a) Hemispherical nucleus of a diameter D; (b) calculated free energy ΔG of a hemispherical nucleus as a function of nucleus diameter D (solid line). A nucleus above the dashed line ($\Delta G = 0$ eV) should not be stable (positive free energy compare to dissociation to vapor) while nucleus with free energy below the dashed line (negative free energy compare to vapor). The smallest stable nucleus at which the free energy becomes negative is at $D = 0.72$ nm; and (c) disk-like nucleus diameter D height H.

TEM image (in agreement with Fig. 2). This process may repeat as long as there is CoF_2 present on the substrate. The larger Co nuclei also grow further and change their overall shape, as dictated by surface energy. Finally, when all CoF_2 is removed, the cobalt crystallites reach a substrate level and then the ripening (coarsening) stage of the exposure starts to take place [Fig. 6(c)].[24,25]

B. Cobalt nucleation and growth

In this section we examine the nucleation and equilibrium shape of cobalt nuclei during the stage depicted in Fig. 6(a). In particular, we would like to identify the critical size of cobalt nucleus (smallest stable nucleus), and understand why the individual particles prefer to grow three dimensionally (3D growth mode). The simple model we would like to introduce assumes that the liberated cobalt atoms have sufficient energy to diffuse over a length comparable to a new nucleus size (2–5 nm).

To estimate the size of cobalt critical nucleus[19] we consider a hemisphere-shaped particle on a flat substrate [Fig. 7(a)]. In this simple model no *a priori* assumptions on crystallographic orientation are made and averaged surface energy values are used. The small observed size of the critical nucleus (<2 nm) and consequent unavailability of crystallographic orientation of such small nuclei necessitates such an approach. For the discussion of the shape of the cobalt particles at the beginning of the ripening stage [Fig. 6(c)] we assume the particles to be disk like. This assumption is based on our diffraction data, HRTEM images, and EFTEM thickness mapping.

Both the size of the critical nucleus and the shape of the cobalt particle depend on the interplay of the various contributions to the free energy. The total difference of free energy ΔG of the aggregating cobalt particle compared to dissociation to vapor can be written as

$$\Delta G = G_{\mathrm{vol}} + G_{\mathrm{surf}} + G_{\mathrm{mag}}, \tag{2}$$

where G_{vol} is the volume free condensation energy, G_{surf} is the surface energy, and G_{mag} is the magnetic energy associated with growth of particles with nonzero magnetization in the strong magnetic field of the objective lens.

The volume free condensation energy (negative) $G_{\mathrm{vol}} = g_{\mathrm{vol}} V$, where g_{vol} is the free energy for unit volume for

cobalt and V is the volume of the particle. For crystalline cobalt at room temperature $g_{\mathrm{vol}} = -230\ \mathrm{eV/nm^3}$.[26] For an initial cobalt particle which is typically a few nanometers in diameter and ~ 1 nm thick the G_{vol} is approximately 1000–2000 eV.

The surface energy term G_{surf} in Eq. (2) involves contributions from the Co–particle interfaces between both the vacuum and substrate. For a hemisphere-shaped particle

$$G_{\mathrm{surf}} = \frac{\pi D^2 \gamma_{\mathrm{Co}}}{2} + \frac{\pi D^2 (\gamma_{\mathrm{Co}} - \gamma_{\mathrm{subst}})}{4}, \tag{3}$$

where D is the diameter of the particle and γ_{Co} and γ_{subst} are the cobalt surface energy and substrate surface energy, respectively. The exact value of the surface energy of a cobalt particle depends on the structure (hcp, fcc, or ϵ-cobalt) and orientation of the particles. The surface energies of hcp cobalt are $\gamma_{100}^{\mathrm{Co}} = 23.75\ \mathrm{eV/nm^2}$ for (100) planes and about $\gamma_{001}^{\mathrm{Co}} = 17.5\ \mathrm{eV/nm^2}$ for (001) planes.[27] For this illustrative estimate we use $\gamma_{\mathrm{Co}} = 20\ \mathrm{eV/nm^2}$ (an average of the above values). We must also take into account the surface energy of the substrate γ_{subst}. We use $\gamma_{\mathrm{subst}} \sim 2\ \mathrm{eV/nm^2}$ as an estimate for CoF_2. Taking about 2–5 nm size initial nucleus the surface energy contribution in G_{surf} is approximately 200–1000 eV.

G_{mag} represents the energy of magnetic cobalt particles growing in the strong magnetic field of the objective lens. We estimate the G_{mag} under the assumption that the particle magnetization (using bulk value 1.7 T) will align the strong field of the objective lens ($B \sim 3$ T). Energy G_{mag} can then be obtained as an energy of a corresponding magnetic dipole in the field of the objective lens. Under such conditions the G_{mag} for a fairly large (5 nm diameter 3 nm thick) particle is about 2 eV. This value corresponds to about 0.1% of G_{vol} and less than 1% of G_{surf}. Magnetic energy G_{mag} is therefore not likely to affect the final shape of the cobalt particles.

Consequently, it is the volume condensation G_{vol} and surface G_{surf} energies that determine the size of the critical nucleus. Neglecting the magnetic term in Eq. (2) the free energy of a hemisphere-shaped nucleus is

$$\Delta G = \frac{\pi D^3 g_{\mathrm{vol}}}{12} + \frac{\pi D^2 \gamma_{\mathrm{Co}}}{2} + \frac{\pi D^2 (\gamma_{\mathrm{Co}} - \gamma_{\mathrm{subst}})}{4} \tag{4}$$

and consequently the diameter D_c of the critical nucleus at which the volume energy starts to overcome surface energy[19] is

$$D_c = \frac{-2(3\gamma_{\mathrm{Co}} - \gamma_{\mathrm{subst}})}{g_{\mathrm{vol}}}, \tag{5}$$

taking values $g_{\mathrm{vol}} = -230\ \mathrm{eV/nm^3}$, $\gamma_{Co} = 20\ \mathrm{eV/nm^2}$, and $\gamma_{\mathrm{subst}} = 2\ \mathrm{eV/nm^2}$ the critical diameter $D_c \sim 0.5$ nm [Fig. 7(b)]. The diameter of the smallest stable nucleus with negative free energy ΔG compared to vapor is $D = 0.72$ nm [Fig. 7(b)]. This is smaller than the smallest diameter of the nuclei we have observed, which is not surprising taking into account limitations of real-time *in situ* observations. It is possible that the observed 2 nm cobalt nuclei are the result of cobalt nucleation on a subnanometer scale. Such nucleation, followed by subsequent crystallographic ordering and growth, leads to nuclei in the ~ 2 nm range which we were able to identify in HRTEM images.

Next we attempt to estimate the energetically favorable shape of a disk-like cobalt particle on an amorphous carbon substrate [Fig. 7(c)]. Taking into account the difficulty of detailed shape calculations and our results of EFTEM thickness mapping in Fig. 6, we approximate the shape of cobalt nuclei by a disk with diameter D and height H as depicted in Fig. 7(b). The most important input parameter in this model is the cobalt surface energy. This energy $G_{\mathrm{surf}}^{z\mathrm{Co}}$ depends on the particular crystallographic orientation. For this illustrative example we chose the top and bottom planes of the disk to be identical with (001) crystallographic planes of hcp cobalt. The surface energy can then be written as

$$G_{\mathrm{surf}} = \frac{\pi}{4} D^2 \gamma_{(001)} + \pi D H \gamma_{(100)} + \frac{\pi}{4} D^2 (\gamma_{(001)} - \gamma_{\mathrm{subst}}), \tag{6}$$

Where D is the diameter of a disk-like nucleus and H is the height (thickness) of such nucleus. Using the expression Eq. (6) for the surface energy contribution and nucleus volume $V_{\mathrm{nucl}} = \pi D^2 H$ we can write the difference of free energy ΔG of the aggregating cobalt particle in Eq. (2) as

$$\Delta G = \frac{\pi D^2 H g_{\mathrm{vol}}}{4} + \frac{\pi}{4} D^2 \gamma_{(001)} + \frac{\pi}{4} D^2 (\gamma_{(001)} + \gamma_{\mathrm{subst}}). \tag{7}$$

To alleviate whether the 3D growth mode is thermodynamically advantageous we calculate the aspect ratio H/D (height over diameter) which minimizes the free energy ΔG for an arbitrary particle volume V. This aspect ratio can be obtained from partial derivatives of Eq. (7) resulting in

$$\frac{H}{D} = \frac{2\gamma_{(001)} - \gamma_{\mathrm{subst}}}{2\gamma_{(100)}}, \tag{8}$$

which for our values of $\gamma_{001} = 17.5\ \mathrm{eV/nm^2}$, $\gamma_{100} = 23.75\ \mathrm{eV/nm^2}$, and $\gamma_{\mathrm{subst}} = 0.63\ \mathrm{eV/nm^2}$ gives $H/D = 0.7$ in good agreement with EFTEM observations in Figs. 4(b) and 5. Equation (8) provides an additional argument for the small influence of the substrate on the film morphology. In other words, the high surface energy of cobalt will force 3D growth for a wide range of substrates. To achieve significant spreading of cobalt the substrate, the energy of the cobalt–substrate interface ($2\gamma_{001}$-γ_{surf},) has to be minimized. In our simple model this means increasing the γ_{surf} to near twice the (already very high) surface energy of cobalt. Equation (8) also suggests the importance of the anisotropy of the cobalt surface energies (difference between γ_{100} and γ_{001}). In the extreme case of large crystalline anisotropy and low substrate surface energy γ_{surf} the particles may minimize their contact with the substrate and the aspect ratio of the particles would be determined by the ratio of the crystalline surface energies. The above conclusions are likely to hold for fcc and ϵ-cobalt (both cubic) unless their surfaces energies are significantly lower than that of hcp cobalt. This simple model provides some insight while avoiding the need to analyze the more complicated situation for hcp cobalt with (100) planes parallel to the substrate, as well as for fcc cobalt and ϵ-cobalt (both cubic).

C. Process parameters and kinetics of the exposure process

The above paragraph discussed the thermodynamically preferred aspect ratio of a cobalt nucleus. The tendency of cobalt to form separated particles rather than a continuous film can be advantageous when one wants to fabricate *in situ* and study sub-10-nm cobalt particles. If the aim is continuous and well-defined structures, then the 3D growth of cobalt particles poses a difficulty. As suggested in the previous paragraph, the driving force for 3D growth is likely the high surface energy of cobalt and the fact that growing cobalt particles ''feel'' the interfacial energy with CoF_2 rather than the substrate until all CoF_2 is removed. Since the equilibrium state is 3D separated nuclei, it is necessary to look to the growth kinetics (and process parameters influencing the kinetics) for ways to control the final morphology. Additionally consideration has to be given to practical process parameters such as carbon and water contamination buildup, oxidation of cobalt, thickness of initial CoF_2, and substrate temperature.

The influence of the substrate temperature during exposure is at least twofold. First, the substrate temperature is an important parameter controlling contamination buildup on the sample.[28,29] Second, change of the substrate temperature can influence fluorine and cobalt diffusion and fluorine desorption from the sample. The (carboneous) contamination buildup during electron beam exposure at room temperature is known to limit the decomposition of alkali halides.[30] This is also the case for exposures in our TEM. The carboneous contamination buildup can be eliminated by either heating or cooling the sample during the exposure process. However at low temperatures the sensitivity of CoF_2 to electron irradiation strongly decreases (Table I) and we have also detected an increased presence of oxygen (presumably water ice) at $T=85$ K. The size of the final particles after exposure was decreased moderately (to about 3–5 nm) at $T=85$ K, but the film retained the separated particle morphology. The decrease of sensitivity likely stems from low diffusion rates of both fluorine and cobalt at $T=85$ K. At elevated temperature ($T=555$ K) the carbonaceous contamination can be avoided completely and the sensitivity of CoF_2 also improves. However increased temperature during exposure leads to formation of somewhat larger cobalt particles, perhaps by promoting cobalt diffusion. Changing the sample temperature between $T\sim 85$ K and $T\sim 700$ K therefore does not seem to promote the desired continuous-cobalt morphology.

The electron-beam current density (dose rate) j is another easily accessible parameter which may influence the final morphology of the exposed film. The current density should primarily influence the rate of fluorine removal and rate of release of free cobalt atoms. The electron beam can also directly remove material by a knock-on mechanism.[31] Finally, in the case of a nonconducting sample (such as CoF_2) the emission of secondary electrons induced by the primary electron beam can lead to charging of the irradiated area. In our microscope it is possible to vary the probe current density over many orders of magnitude. However, as mentioned previously, dose rates in excess of ~ 1200 A/cm^2 lead to removal of both fluorine and cobalt from the exposed area (leaving bare substrate behind). This sets the upper limit for useable dose rates. Decreasing the dose rate leads to increased sensitivity of CoF_2 (decrease in characteristic dose D_e in Table I). The decrease in D_e however is not large enough to make up for the need to expose longer to deliver a sufficient dose to remove fluorine from the exposed area. It is therefore advantageous to expose the film at a high dose rate, limited by removal of Co from the exposed area. It is difficult to comment on the beam-induced heating and beam-induced electrostatic charging. It is perhaps worth mentioning that a moderate charging of the sample can lead to strong repulsive forces between cobalt nuclei on a CoF_2 substrate (and consequently to promotion of growth of separated nuclei rather than of continuous structures).

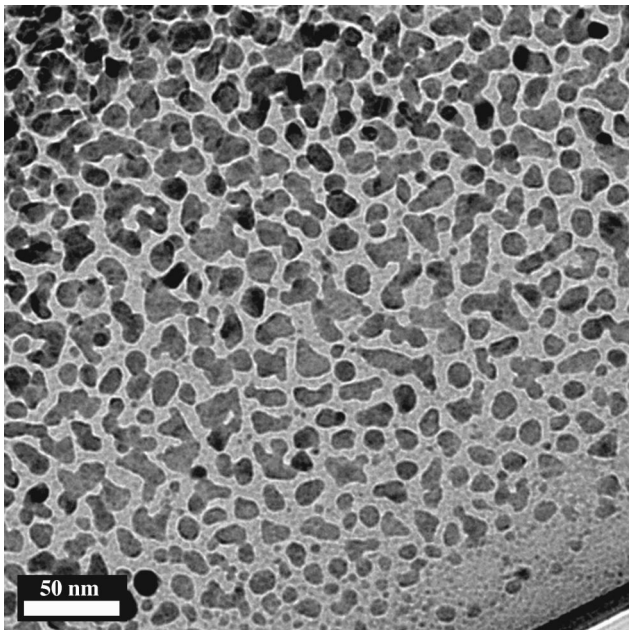

FIG. 8. Influence of the thickness of the initial CoF_2 film on the morphology of the film after complete exposure. The thickness of the initial CoF_2 film increased from the bottom right corner (less than 8 nm of initial CoF_2) toward the upper left corner (~ 20 nm of initial CoF_2). The increase in CoF_2 thickness leads to more frequent overlap of cobalt crystallites after exposure rather than in continuous cobalt film. The scale bar corresponds to 50 nm.

The influence of the sample thickness is illustrated in Fig. 8. The CoF_2 initial film thickness increased from the bottom-right corner toward the top-left corner. The area was uniformly exposed, with a dose approximately corresponding to the onset of the ripening stage. The figure reveals that the size of the particles is about 10–15 nm over the whole area of the film, with the exception of the very right bottom corner where the initial CoF_2 film was thinnest. Increasing the CoF_2 thickness (toward the top left corner) leads to increased frequency of overlap between particles rather than an increase of particle size. This is in agreement with the qualitative model in Sec. V A. The area of the thinnest initial CoF_2 film (right bottom corner) leads to separated cobalt particles with very little overlap. Such nonoverlapping particles on a bare substrate appear to be suitable for electron-holography measurements of magnetization of such particles. No apparent change in HRTEM images of such particles was observed

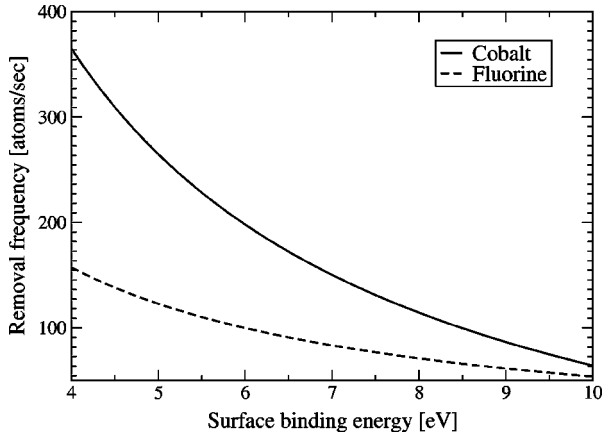

FIG. 9. Rate of cobalt and fluorine atoms removal as a function of surface binding energy for current density $j=220$ A/cm^2.

at doses more than 10^4 C/cm^2, suggesting sufficient stability for the holography experiments.

It is perhaps worthwhile to estimate the rate of cobalt and fluorine removal by a knock-on mechanism during electron beam exposure. The energy transferred to an atom by the knock-on mechanism $E_{\max}$[31,32] can be estimated using (in eV) $E_{\max}=E_0(E_0+1022)/(460A)$ where A is atomic weight and E_0 is incident electron energy in keV. For fluorine and 300 keV electron beam $E^F_{\max}=45$ eV; and for cobalt $E^{\mathrm{Co}}_{\max}=14.6$ eV. It is also possible to estimate the frequency of removal of fluorine f^F and cobalt f^{Co} as a function of surface binding energy E_s using[31]

$$f=jZ^2\frac{3.54\times10^{-17}}{eAE_0}\left(\frac{1}{E_s}-\frac{1}{E_{\max}}\right), \tag{9}$$

where f is in atoms/s, j is the dose rate in A/cm^2, Z is the atomic number, A is the atomic weight, e is the electron charge, E_s is the surface binding energy in eV of the atom of interest, and $E_{\max}$ is the maximum energy transferred by the knock-on mechanism. Figure 9 shows the relation as a function of E_s for $j=220$ A/cm^2. This figure suggests that about three times as many Co atoms compared to F are removed by the knock-on mechanism if F and Co have the same binding energy. For j below 1200 A/cm^2 the fluorine is removed from the beam area. Figure 9 implies that either the binding energy of cobalt is greater than for F or that (at least for $j<1200$ A/cm^2) the knock-on removal is not the determining mechanism for F or Co removal. This is in agreement with the previous studies[33,34] where electron-stimulated desorption was identified as the removal mechanism of halide atoms. The energy delivered by the knock-on transfer can, however, promote surface diffusion of cobalt. The stability of the separated cobalt particles mentioned above confirms that the knock-on mechanism is rather unimportant for existing cobalt particles.

Finally we address the influence of the presence of oxygen and water vapor on the exposure process. At low temperature ($T=85$ K) the water is mostly present as an ice layer on the sample. Such an ice layer may influence the exposure process in a way very similar to carboneous contamination at room temperature: reducing the CoF_2 sensitivity by blocking the fluorine diffusion from the sample. At room temperature, as well as elevated temperature, water (and molecular oxygen) is a likely source of oxygen for the formation of cobalt oxides within the film. A rough estimate (Ref. 19, page 1–21) suggests that approximately 5×10^{13} cm^{-2} s^{-1} H_2O and 3.6×10^{13} cm^{-2} s^{-1} oxygen molecules reach the sample during exposure at $T=300$ K in a typical microscope vacuum in the sample area ($\sim10^{-7}$ Torr). It is likely that due to electron-beam irradiation a large portion of the water and oxygen will be present in the highly reactive, excited state.

VI. CONCLUSIONS

Direct electron-beam exposure of CoF_2 is a promising way to produce magnetic cobalt structures on a length scale of a few nanometers. However, many issues still have to be addressed. Our findings reveal that elevated substrate temperature during the exposure enables complete removal of fluorine from the exposed area and leads to increased electron-beam sensitivity of CoF_2. The exposed area was composed of separated cobalt particles on a bare substrate, rather than a continuous cobalt structures. This behavior was not altered by changing the dose rate j or substrate temperature T. The influence of the substrate on the growing patterns is absent until the final stages of exposure, when CoF_2 is completely removed and cobalt particles come into contact with the substrate. Increased dose rate j leads to an increase in the characteristic dose D_e for fluorine removal, suggesting a diffusion-limited exposure process. High dose rates ($j>1200$ A/cm^2) lead to removal of both fluorine and cobalt from the exposed area, leaving a bare substrate within the beam. A lower temperature during exposure reduces the CoF_2 sensitivity, while retaining the limiting dose rate ($j<1200$ A/cm^2) which can be used without removing cobalt from the exposed area. Increasing the initial CoF_2 thickness results in an increased overlap of Co crystallites, rather than to continuous cobalt structures. Adjusting the thickness of the initial CoF_2 film allowed us to prepare samples of well-separated, single-crystal cobalt particles with size about 2–15 nm. Such individual particles prepared on a thin amorphous substrate appear to be suitable for mapping of the magnetic field by electron holography experiments. The technique however does not seem to be suitable for fabrication of devices where continuous magnetic films are needed.

ACKNOWLEDGMENTS

This work was supported under the Division of Materials Sciences, U.S. Department of Energy, under Contract No. DE-AC02-98CH10886. The authors would like to acknowledge frequent discussion with Dr. Laura H. Lewis, Dr. Joe Wall, Lijun Wu, and Dr. Mark Freeman. The help and advice of Bob Sabatini and Arnie Moodenbaugh is also deeply appreciated.

[1] R. P. Cowburn and M. E. Welland, Science **287**, 1446 (2000).
[2] R. H. Kodama, J. Magn. Magn. Mater. **200**, 359 (1999).
[3] D. Streblechenko and M. R. Scheinfein, J. Vac. Sci. Technol. A **16**, 1374 (1998).

[4] H. C. Manoharan, C. P. Lutz, and D. Eigler, Nature (London) **403**, 512 (2000).
[5] S. W. Hla, L. Bartels, G. Meyer, and K. H. Reider, Phys. Rev. Lett. **85**, 2777 (2000).
[6] A. Hubert and R. Schafer, *Magnetic Domains: The Analysis of Magnetic Microstructures* (Springer, New York, 1998).
[7] M. R. Freeman, J. Appl. Phys. **75**, 6194 (1994).
[8] W. K. Hiebert, PhD thesis, University of Alberta, Alberta, Canada, 2001.
[9] M. Al-Khafaji, W. M. Rainforth, M. R. J. Gibbs, J. E. L. Bishp, and H. A. Davies, J. Appl. Phys. **83**, 6441 (1998).
[10] Y. Aharonov and D. Bohm, Phys. Rev. **115**, 485 (1959).
[11] A. Tonomura, *Electron Holography* (Springer, New York, 1993).
[12] M. De Graef and Y. Zhu, *Magnetic Imaging and its Applications to Materials* (Academic, New York, 2001).
[13] E. Völkl, L. F. Allard, and D. C. Joy, *Introduction to Electron Holography* (Plenum, New York, 1999).
[14] R. Messier, A. P. Giri, and R. A. Roy, J. Vac. Sci. Technol. A **2**, 500 (1984).
[15] S. G. Bales, R. Bruinsma, E. A. Eklund, R. P. U. Karunasiri, J. Rudnick, and A. Zangwill, Science **249**, 264 (1990).
[16] R. F. Egerton, *Electron Energy-Loss Spectroscopy in the Electron Microscope*, 2nd ed. (Plenum, New York, 1996).
[17] G. S. Chen and C. J. Humphreys, J. Vac. Sci. Technol. B **15**, 1954 (1997).
[18] R. Zanetti, A. L. Bleloch, M. P. Grimshaw, and G. A. Jones, Philos. Mag. Lett. **69**, 285 (1994).
[19] L. I. Maissel and R. Glang, *Handbook of Thin Film Technology* (McGraw-Hill, New York, 1970).
[20] K. B. Alexander, P. F. Becher, S. B. Waters, and A. Bleier, J. Am. Ceram. Soc. **77**, 939 (1994).
[21] R. F. Egerton and I. Rauf, Ultramicroscopy **80**, 247 (1999).
[22] H. Sato, O. Kitakami, T. Sakurai, Y. Shimada, Y. Otani, and K. Fukamichi, J. Appl. Phys. **81**, 1858 (1997).
[23] S. Sun and B. C. Murray, J. Appl. Phys. **85**, 4325 (1999).
[24] Centre D'Information du Cobalt, Cobalt Monograph, Brussels, Belgium 1960.
[25] P. Avouris, R. Kawai, N. D. Lang, and D. M. Newns, J. Chem. Phys. **89**, 2388 (1988).
[26] *Selected Values of Thermodynamic Properties of Metals and Alloys*, edited by P. D. Anderson, and K. K. Kelly (Wiley, New York, 1963), pp. 74–80.
[27] L. Vitos, A. V. Ruban, H. L. Skriver, and J. Kollar, Surf. Sci. **411**, 186 (1998).
[28] J. S. Wall, *Proceedings of Scanning Electron Microscopy* 1980 (SEM Inc. AMF O'Hare, Chicago, IL).
[29] J. J. Hren, J. J. Goldstein, and C. David, *Introduction to Analytical Electron Microscopy* (Plenum, New York, 1979).
[30] J. Fujita, H. Watanabe, Y. Ochiai, S. Manako, J. S. Tsai, and S. Matsui, J. Vac. Sci. Technol. B **13**, 2757 (1995).
[31] R. Egerton, P. A. Crozier, and P. Rice, Ultramicroscopy **23**, 305 (1987).
[32] L. T. Chadderton, *Radiation Damage in Crystals* (Methuen, London, 1965).
[33] T. E. Madey, Science **234**, 316 (1986).
[34] P. D. Townsend and J. C. Kelly, Phys. Lett. **26A**, 138 (1968).